Astrophysics and Space Science (2024) 369:1
https://doi.org/10.1007/s10509-023-04263-6

RESEARCH

Properties of relativistic hot accretion flow around a rotating black hole with radially varying viscosity

Monu Singh[1] · **Santabrata Das**[1]

Received: 4 July 2023 / Accepted: 18 December 2023

Abstract
We examine the effect of the variable viscosity parameter (α) in relativistic, low angular momentum advective accretion flow around rotating black holes. Following the recent simulation studies of the magnetohydrodynamic disk that reveal the radial variation of $\alpha(r)$, we theoretically investigate the properties of the global transonic accretion flow considering a one-dimensional power-law prescription of the viscosity parameter as $\alpha(r) \propto r^{\theta}$, where the viscosity exponent θ is a constant. In doing so, we adopt the relativistic equation of state and solve the fluid equations that govern the flow motion inside the disk. We find that depending on the flow parameters, accretion flow experiences centrifugally supported shock transitions and such shocked accretion solutions continue to exist for wide ranges of the flow energy, angular momentum, accretion rate, and viscosity exponent, respectively. Due to shock compression, the hot and dense postshock flow (hereafter PSC) can produce the high-energy radiations after reprocessing the soft photons from the preshock flow via inverse Comptonization. Since PSC is usually described using shock radius (r_s), compression ratio (R), and shock strength (S), we study the role of θ in detemining r_s, R, and S, respectively. Moreover, we obtain the parameter space for a shock and find that the possibility of shock formation diminishes as θ is increased. Finally, we compute the limiting value of θ (*i.e.*, $\theta^{\max}$) that admits a shock and find that flow can sustain more viscosity when it accretes onto a rapidly rotating ($a_{\rm k} \to 1$) black hole in comparison to a weakly rotating ($a_{\rm k} \to 0$) black hole.

Keywords accretion · accretion disk · black hole physics · hydrodynamics · shock waves

1 Introduction

Accretion of matter onto a compact object is considered to be the most efficient energy-release process. However, in the context of accretion disk theory, the underlying mechanisms responsible for transporting the angular momentum through the disk are not yet well understood and remain the most intriguing unresolved problem due to the disagreement of findings between the numerical simulations (Balbus and Hawley 1998) and observational results (Smak 1999). In particular, King et al. (2007) found an apparent discrepancy of a factor of ~ 10 between observational and theoretical estimates of the viscosity parameter in accretion flow around a black hole (BH).

In a seminal work, Shakura and Sunyaev (1973) (hereafter SS73) introduced the dimensionless viscosity parameter α defined as the ratio of the viscous stress to the pressure of the accretion flow. In the absence of a detailed understanding of the viscous mechanism, SS73 considered α to be a global constant throughout, typically in the range 0.001–0.1 (Das et al. 2021, and references therein). Then, considering the effective shear viscosity driven by the magnetorotational instability, Hawley and Krolik (2001, 2002) suggested that α may not be constant throughout the flow, instead it possibly varies both spatially and temporally in an accretion flow. Similar findings were also reported by numerous groups of researchers while examining the overall characteristics of α using magnetohydrodynamical simulations (Balbus and Hawley 1991; Matsumoto and Tajima 1995; Hawley et al. 1995, 1996; Lyubarskii 1997; Nayakshin 1999; Steinacker and Papaloizou 2002; Sano et al. 2004; Fragile et al. 2007; Penna et al. 2010, 2012; Porth

✉ S. Das
sbdas@iitg.ac.in

M. Singh
monu18@iitg.ac.in

[1] Department of Physics, Indian Institute of Technology Guwahati, Guwahati, 781039, Assam, India

Published online: 05 January 2024

et al. 2019). Very recently, Mitra et al. (2022) computed the profile of the ratio of Maxwell stress to the gas pressure, and found that unlike the standard SS73 viscosity parameter, it also varies with radial distance as well. Clearly, the measure of α from both local and global simulations is undoubtedly challenging as it depends on several factors, namely the initial magnetic-field geometry and strength, grid resolutions, etc. (Sorathia et al. 2012). Accordingly, it appears that the range of α values is not well constrained and hence, it remains inconclusive.

Indeed, it is the viscous stress that generally varies inside the disk, and hence, α is often considered as radially varying. Adopting these ideas, we investigate the properties of relativistic viscous advective accretion flow around the rotating BHs. During accretion, matter starts accreting with subsonic speed from a large distance and plunges into the BH supersonically to meet the horizon condition. Due to this, inflowing matter experiences a smooth transition from the sub- to the supersonic domain at least once while accreting onto BH. However, flow can encounter such sonic transitions multiple times depending on the flow energy and angular momentum, and a solution of this kind is specially encouraging because a centrifugal wall may trigger shock transitions (Fukue 1987; Chakrabarti 1989; Abramowicz and Chakrabarti 1990; Yang and Kafatos 1995; Das et al. 2001,b; Chakrabarti and Das 2004; Das 2007; Kumar and Chattopadhyay 2014; Sarkar and Das 2016; Das and Sarkar 2018; Dihingia et al. 2018, 2019a,b; Das et al. 2021; Sen et al. 2022; Patra et al. 2022). Such shock transitions are possible provided the Rankine–Hugoniot conditions (RHCs) are favorable (Landau and Lifshitz 1959). At a shock, accreting matter jumps from supersonic to subsonic values and this causes the convergent postshock matter to be hot, dense, and puffed-up, which is commonly referred as postshock corona (PSC). After the shock, accreting matter starts moving towards the horizon and gradually gains radial velocity. This process continues and finally, matter crosses the event horizon (r_g) with supersonic speed after passing through a critical point located close to r_g. In reality, PSC comprises a swarm of the hot electrons. These electrons interact with the soft photons from preshock matter via an inverse-Comptonization process and produce hard X-ray radiations (Chakrabarti and Titarchuk 1995; Mandal and Chakrabarti 2005). When RHCs are not satisfied, however, flow possesses more than one critical point, PSC is expected to exhibit time-varying modulation that usually may give rise to the quasiperiodic variations of emitted photons commonly observed from Galactic BH sources (Chakrabarti and Manickam 2000; Nandi et al. 2001, 2012; Majumder et al. 2022; Das et al. 2021, and references therein).

Being motivated by this, we examine the structure of the steady, viscous, advective flow that accretes onto a rotating BH. We adopt the viscosity parameter that is radially varying as $\alpha(r) = \alpha_0(r/r_g)^\theta$, where r is the radial distance, r_g is gravitational radius, α_0 is the proportionality constant, and θ is the viscosity exponent. We consider the relativistic equation of state (REoS) that satisfactorily accounts for the thermal properties of the low angular momentum accreting matter (Chattopadhyay and Ryu 2009; Dihingia et al. 2019a). Further, we use a recently developed pseudopotential to mimic the BH gravity (Dihingia et al. 2018) for spin values ranging from weakly rotating ($a_k \to 0$) to rapidly rotating ($a_k \to 1$) limits. Considering all these, we calculate the global transonic accretion solutions (GTAS) by solving the fluid equations using the accretion model parameters. Moreover, we identify the requisite GTAS that admit standing shock transitions, and render the dependencies of the dynamical as well as thermodynamical flow variables on the model parameters. In addition, we investigate the various shock properties, such as shock radius (r_s), compression ratio (R), and shock strength (S), respectively, and study how r_s, R, and S depend on the viscosity (α) and accretion rate ($\dot{m}$). We also determine the range of flow energy ($\mathcal{E}$) and angular momentum (λ) that render shock-induced GTAS, and ascertain the domain of shock-parameter space in the $\lambda - \mathcal{E}$ plane. We find that such a parameter space is altered as the viscosity exponent (θ) is varied. Since θ plays a pivotal role in deciding the accretion disc structure, it is important to explore the limiting value of the viscosity exponent ($\theta^{\max}$). Accordingly, we put effort into estimating $\theta^{\max}$ and find that it strongly depends on both BH spin (a_k) and α_0.

This paper is organized in the following manner. In Sect. 2, we describe the model considerations and basic equations. We obtain GTAS both in the absence and presence of shock and discuss the shock properties in Sect. 3. In Sect. 4, we discuss how the shock-parameter space alters with the change of viscosity and calculate the maximum limit of the viscosity exponent for shocks. Finally, in Sect. 5, we present some conclusions.

2 Basic considerations and model equations

We begin with an axisymmetric, steady-state, height-averaged viscous advective accretion disk around a rotating BH in the presence of synchrotron cooling. We also consider that such a disk remains confined around the disk equatorial plane. We approximate the effect of gravity by adopting an effective pseudopotential (Dihingia et al. 2018) that successfully delineates the space–time wrapping due to a rotating BH. The accretion process inside the disk is driven by the viscous stress ($W_{r\phi}$) and we consider $W_{r\phi} = -\alpha\Pi$, where Π denotes the vertically integrated pressure including ram pressure, and α, the viscosity parameter, is the dimensionless quantity that is assumed to vary with the radial coordinate. Note that α absorbs all the detailed microphysics

of the viscous processes. With these considerations, we express all the governing equations using $M_{\rm BH} = G = c = 1$, where $M_{\rm BH}$, G, and c denote BH mass, gravitational constant, and light speed, respectively. With this, we write the length in units of $r_g = GM_{\rm BH}/c^2$, and accordingly, time and angular momentum are written in units of r_g/c and $r_g c$.

2.1 Governing equations

The basic fluid equations that describe the motion of the accreting matter inside the disc around a rotating BH are as follows:

(a) Conservation equation for radial momentum:

$$\upsilon\frac{d\upsilon}{dr} + \frac{1}{h\rho}\frac{dP}{dr} + \frac{d\Phi_{\rm e}^{\rm eff}}{dr} = 0, \tag{1}$$

where υ, P, ρ, and h, denote the flow velocity, gas pressure, mass density, and specific enthalpy, respectively. In addition, $\Phi_{\rm e}^{\rm eff}$ refers to the effective potential of a rotating BH that mimics the space–time geometry at the disc equatorial plane and is given by (Dihingia et al. 2018),

$$\Phi_{\rm e}^{\rm eff} = \frac{1}{2}\ln\left[\frac{r\Delta}{a_{\rm k}^2(r+2) - 4a_{\rm k}\lambda + r^3 - \lambda^2(r-2)}\right], \tag{1a}$$

where λ is the specific angular momentum of the accreting matter, $a_{\rm k}$ denotes the BH spin, and $\Delta = r^2 - 2r + a_{\rm k}^2$.

(b) Mass-conservation equation:

$$\dot{M} = 2\pi\upsilon\Sigma\sqrt{\Delta}\,, \tag{2}$$

where $\dot{M}$ is the mass accretion rate. In this work, we do not consider the ejection of matter in the form of outflow/jets and hence, $\dot{M}$ is treated as a global constant in the absence of any mass loss from the disk. Moreover, for convenience, we express the accretion rate in units of Eddington accretion rate as $\dot{m} = \dot{M}/\dot{M}_{\rm Edd}$, where $\dot{M}_{\rm Edd} = 1.44 \times 10^{17}\left(\frac{M_{\rm BH}}{M_\odot}\right)$. Further, Σ is the vertically integrated surface mass density of the accreting matter (Matsumoto et al. 1984), and is written as $\Sigma = 2\rho H$, where H refers the local disc half-thickness expressed as (Riffert and Herold 1995; Peitz and Appl 1997),

$$H^2 = \frac{Pr^3}{\rho\mathcal{F}},\ \mathcal{F} = \gamma_\phi^2\frac{(r^2+a_{\rm k}^2)^2 + 2\Delta a_{\rm k}^2}{(r^2+a_{\rm k}^2)^2 - 2\Delta a_{\rm k}^2},\ \gamma_\phi^2 = \frac{1}{(1-\lambda\Omega)}\,.$$

Here, $\Omega\left[=(2a_{\rm k} + \lambda(r-2))/(a_{\rm k}^2(r+2) - 2a_{\rm k}\lambda + r^3)\right]$ denotes the angular velocity of the accreting matter.

(c) Conservation equation for azimuthal momentum:

$$\upsilon\frac{d\lambda}{dr} + \frac{1}{\Sigma r}\frac{d}{dr}(r^2 W_{r\phi}) = 0, \tag{3}$$

where we consider the $r\phi$ component of the viscous stress as $W_{r\phi} = -\alpha\Pi = -\alpha(W + \Sigma\upsilon^2)$ (Chakrabarti and Molteni 1995; Chakrabarti and Das 2004, and references therein). In equation (3), W denotes the vertically integrated pressure and Σ represents the vertically integrated mass density. In this work, we consider a radially varying viscosity parameter resembling a power-law distribution as

$$\alpha = A\left(\frac{r}{r_g}\right)^\theta = \alpha_0 r^\theta, \tag{3a}$$

where A, θ, and α_0 are regarded as constants throughout the flow. Similar findings on the radial variation of the viscosity parameter were also recently reported by several workers (Penna et al. 2013; Zhu and Stone 2018). Note that when $\theta \to 0$, we obtain the globally constant viscosity parameter $\alpha = \alpha_0$, as in the case of 'α model' prescription (Shakura and Sunyaev 1973).

(d) Equation for energy balance:

$$\Sigma\upsilon T\frac{ds}{dr} = \frac{\upsilon H}{\Gamma - 1}\left(\frac{dP}{dr} - \frac{\Gamma P}{\rho}\frac{d\rho}{dr}\right) = Q^- - Q^+. \tag{4}$$

In equation (4), T is the flow temperature, s is the specific entropy, and Γ is the adiabatic index. Moreover, during accretion, the heat gained and lost by the flow are denoted by Q^+ and Q^-, respectively. Following Chakrabarti (1996), Aktar et al. (2017), we adopt the mixed shear-stress prescription to compute the viscous heating of the flow and is given by:

$$Q^+ = -\alpha\rho H r\left(\frac{P}{\rho} + \upsilon^2\right)\frac{d\Omega}{dr}. \tag{5}$$

In general, the bremsstrahlung cooling process is regarded as an inefficient cooling process (Chattopadhyay and Chakrabarti 2000). Hence, in this work, we consider energy loss due to synchrotron cooling only. Accordingly, the synchrotron emissivity of the convergent accretion flow is obtained as (Shapiro and Teukolsky 1983),

$$Q^- = Q^{\rm syn} = \frac{16}{3}\frac{e^2}{c}\left(\frac{eB}{m_e c}\right)^2\left(\frac{k_B T}{m_e c^2}\right)^2 n_e \text{ erg cm}^{-3}\text{ s}^{-1}, \tag{6}$$

where e, m_e, and n_e are the charge, mass, and number density of the electrons, respectively, k_B is the Boltzmann constant, B is the magnetic field. In the astrophysical context, the present of magnetic fields is ubiquitous inside the disc and hence, the ionized flow should emit synchrotron photons causing the accreting flow to cool significantly. Indeed, the characteristics of structured magnetic fields inside the disc still remains unclear, and hence, we rely on the random or stochastic magnetic field. For the purpose of simplicity, we use equipartition to estimate the magnetic field and it is obtained as $B = \sqrt{8\pi\beta P}$, where β is a dimensionless constant. Evidently, $\beta \lesssim 1$ confirms that the magnetic fields remain

confined within the accretion disc (Mandal and Chakrabarti 2005). For the purpose of representation, in this work, we choose $\beta = 0.1$.

In order to close the governing equations (1)–(4), one requires to consider an equation of state (EoS) that relates P, ρ, and internal energy (ϵ) of the flow. Hence, we consider an EoS for relativistic flow that is given by (Chattopadhyay and Ryu 2009),

$$\epsilon = \frac{\rho f}{\left(1 + \frac{m_p}{m_e}\right)}, \tag{7}$$

with

$$f = \left[1 + \Theta\left(\frac{9\Theta + 3}{3\Theta + 2}\right)\right] + \left[\frac{m_p}{m_e} + \Theta\left(\frac{9\Theta m_e + 3m_p}{3\Theta m_e + 2m_p}\right)\right],$$

where Θ $(= k_B T/m_e c^2)$ is the dimensionless temperature of the flow. Utilizing the relativistic EoS, we express the polytropic index as $N = \frac{1}{2}\frac{df}{d\Theta}$, the adiabatic index as $\Gamma = 1 + 1/N$, and the sound speed as $C_s^2 = \frac{\Gamma P}{e+P} = \frac{2\Gamma\Theta}{f+2\Theta}$, respectively (Mitra et al. 2022, and references therein). Further, following Chattopadhyay and Kumar (2016) and with the help of equation (2), we compute the entropy accretion rate as $\dot{\mathcal{M}} = \upsilon H\sqrt{\Delta}\left[\Theta^2(2+3\Theta)\left(3\Theta + 2m_p/m_e\right)\right]^{3/4} \times \exp(k_1)$, where $k_1 = 0.5 \times \left[f/\Theta - (1 + m_p/m_e)/\Theta\right]$.

Using equations (1)–(7), we obtain the radial velocity gradient in the form of a wind equation as,

$$\frac{d\upsilon}{dr} = \frac{\mathcal{N}(r, \upsilon, \Theta, \lambda, \alpha)}{\mathcal{D}(r, \upsilon, \Theta, \lambda, \alpha)}, \tag{8}$$

where both $\mathcal{N}$ and $\mathcal{D}$ depend on r, υ, Θ, λ, α, and their explicit mathematical expressions are given in the Appendix. Using equation (8), we obtain the radial derivatives of angular momentum (λ) and dimensionless temperature (Θ) as,

$$\frac{d\lambda}{dr} = \lambda_1 + \lambda_2\frac{d\upsilon}{dr} \tag{9}$$

and

$$\frac{d\Theta}{dr} = \Theta_1 + \Theta_2\frac{d\upsilon}{dr}, \tag{10}$$

where the mathematical forms of the coefficients, such as λ_1, λ_2, Θ_1, and Θ_2 are described in the Appendix.

Indeed, during accretion, subsonic flow commences accreting towards the BH from a far-away distance $r_{\rm edge}$ (hereafter, the disc outer edge) and crosses the BH horizon (r_h) supersonically. Therefore, flow ought to pass through a critical point (r_c) where it smoothly transits from a subsonic to a supersonic domain. Note that for $r > r_h$, flow may possess multiple critical points depending on the flow parameters. Following Chakrabarti and Das (2004), we carry out the critical-point analysis, where $\left(\frac{d\upsilon}{dr}\right)_{r_c} = \frac{0}{0}$ as one obtains $\mathcal{N} = \mathcal{D} = 0$ at the critical point. Due to this, we make use of the l´Hospital rule while computing $\left(\frac{d\upsilon}{dr}\right)$ at r_c. For physically acceptable solutions around BH, we consider saddle-type critical points only where $\left(\frac{d\upsilon}{dr}\right)$ yields two distinct real values at the critical point (Das 2007, and references therein). When r_c forms near r_h, we refer to it as the inner critical point ($r_{\rm in}$), otherwise it is termed the outer critical point ($r_{\rm out}$) (Chakrabarti and Das 2004).

3 Global transonic accretion solutions (GTAS)

The global transonic accretion solutions (GTAS) are obtained by solving the coupled differential equations (8)–(10) for a set of model parameters. Some of these parameters, namely α_0, θ, $\dot{m}$, and $a_{\rm k}$ remain constant throughout, while the others, *i.e.*, the critical point r_c and angular momentum λ_c at r_c are treated as local parameters. Using the model parameters, we first integrate equations (8)–(10) starting from r_c up to r_h and again from r_c to $r_{\rm edge}$ (∼1500). Thereafter, a complete GTAS around BH is obtained by joining both parts of the solutions. Based on the choice of the model parameters, flow becomes transonic either at $r_{\rm in}$ or at $r_{\rm out}$ before crossing the BH horizon.

Figure 1 shows the typical sets of global transonic accretion solutions (GTAS) for flows injected from $r_{\rm edge} = 1500$ with various θ values. Following the procedure mentioned in Das (2007), we calculate the accretion solution containing the inner critical point $r_{\rm in} = 5.50$, where we choose $\lambda_{\rm in} = 3.15$, $\alpha_0 = 0.01$, $\theta = 0.0$, $a_{\rm k} = 0.0$, and $\dot{m} = 0.01$. This renders a global accretion solution as it successfully connects the BH horizon r_h with $r_{\rm edge}$. We note the flow

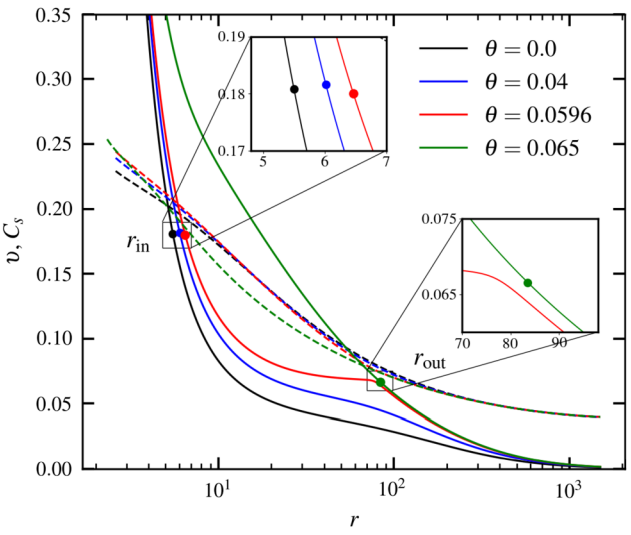

Fig. 1 Plot of flow velocity (υ) and sound speed (C_s) with radial distance (r) for different values of θ. Dashed curves represent the sound speed and solid curves denote flow velocity. See the text for details

Table 1 Power-law exponent (θ), critical-point location (r_c), critical-point angular momentum (λ_c), critical-point velocity (υ_c), critical-point temperature (Θ_c), disk outer edge (r_{edge}), angular momentum at r_{edge} (λ_{edge}), velocity at r_{edge} (υ_{edge}), temperature at r_{edge} (Θ_{edge}) for global transonic solutions presented in Fig. 1. See the text for more details

θ	r_c (r_g)	λ_c ($r_g c$)	υ_c (c)	Θ_c ($m_e c^2 K$)	r_{edge} (r_g)	λ_{edge} ($r_g c$)	υ_{edge} (c)	Θ_{edge} ($m_e c^2 K$)
0	5.50	3.15	0.1808	27.9476	1500.0	21.10	0.00089	0.98115
0.04	6.019	3.03	0.1816	28.2146	1500.0	21.10	0.00118	0.98106
0.0596	6.464	2.96	0.1800	27.6714	1500.0	21.10	0.00137	0.98099
0.065	83.488	2.83	0.0665	3.4779	1500.0	21.10	0.00140	0.98098

Note: Suffix 'c' identifies quantities measured at the inner (outer) critical point r_{in} (r_{out}).

variables at r_{edge} as $\lambda_{edge} = 21.10$, $\upsilon_{edge} = 8.9 \times 10^{-4}$, and $\Theta_{edge} = 0.98115$. In reality, we can obtain the same accretion solution once the flow equations are integrated towards the BH horizon using these noted boundary values. Here, black solid curves denote the radial velocity $\upsilon(r)$, whereas black dashed curves represent the sound speed $C_s(r)$ of the flow for $\theta = 0.0$. Next, we increase $\theta = 0.04$ while keeping other flow variables unchanged at r_{edge} and calculate GTAS by suitably tuning $\upsilon_{edge} = 1.18 \times 10^{-3}$, and $\Theta_{edge} = 0.98106$. Here, we additionally require the boundary values of υ_{edge} and Θ_{edge} to integrate the fluid equations from r_{edge}, as the critical point remains unknown. The solution is depicted using blue color where we find that the inner critical point is shifted outwards as $r_{in} = 6.019$ for $\theta = 0.04$. Similarly, for $\theta = 0.0596$, the flow solution (red) continues to maintain similar character as in the case of $\theta = 0.0$ and 0.04, having inner critical points at $r_{in} = 6.464$. Solutions of this kind that are passing through r_{in} are similar to ADAF-type accretion solutions (Narayan and Yi 1994). When θ is increased further, the nature of the flow solution (in green) is changed and it becomes transonic at the outer critical point $r_{out} = 83.488$ rather than r_{in}. When θ is increased further, the flow solution (in green) changes its character and becomes transonic at the outer critical point $r_{out} = 83.488$ instead of the inner critical point. Usually, the solutions containing r_{out} are of Bondi-type (Bondi 1952). For the purpose of clarity, regions around the critical points (r_{in} and r_{out}) are zoomed, which are shown using filled circles at the insets. We tabulate the flow variables at r_{edge}, r_{out}, and r_{in} in Table 1. Overall, we observe that the role of θ is pivotal in deciding the characteristic of GTAS around BHs.

Next, we present the accretion flow solutions in Fig. 2a, where the radial variation of Mach number ($M = \upsilon/C_s$) is demonstrated. Here, all the solutions become transonic at $r_{in} = 6.17$ with $\lambda_{in} = 3.01$, $\alpha_0 = 0.01$, $\dot{m} = 0.01$, $a_k = 0.0$, respectively. For $\theta = 0.6$, we obtain a GTAS that smoothly connects the BH horizon with r_{edge} where the flow angular momentum matches with its Keplerian value, as shown in the dotted curve. We gradually decrease θ and find that

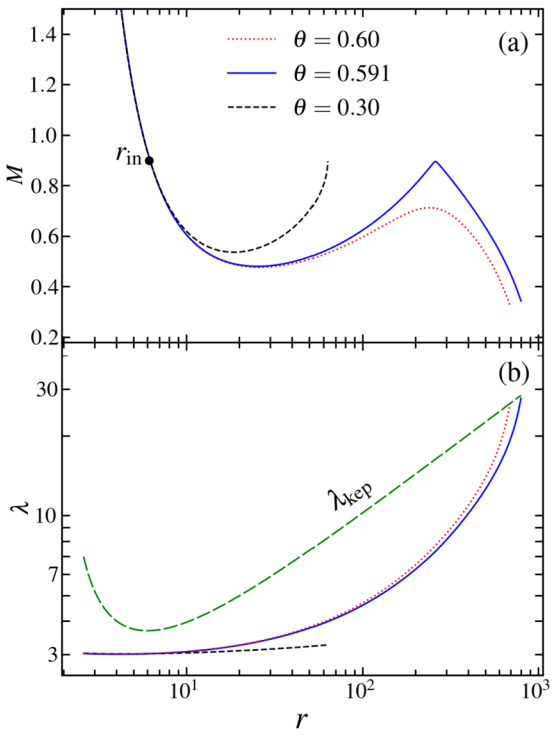

Fig. 2 Variation of (a) Mach number M ($= \upsilon/C_s$) and (b) angular momentum (λ) with the radial distance r for different θ. Here, we choose $r_{in} = 6.17$, $\lambda_{in} = 3.01$, $\alpha_0 = 0.01$, and $\dot{m} = 0.01$. Dashed, solid, and dotted curves denote results for $\theta = 0.30$, 0.591, and 0.60, respectively. See the text for details

beyond the limiting value as $\theta = 0.591$, accretion flow becomes closed, as shown in the solid curve. The result plotted using a dashed curve corresponds to $\theta = 0.3$. The closed accretion solutions passing through r_{in} are noteworthy as they can join with another solution passing through r_{out} via centrifugally supported shocks. Indeed, the existence of shocks in advective accretion flows has intense implications because the solution of this kind satisfactorily explains the temporal and spectral properties of BH sources (Molteni et al. 1994, 1996; Chakrabarti and Titarchuk 1995; Chakrabarti 1996; Lu et al. 1999; Chakrabarti and Man-

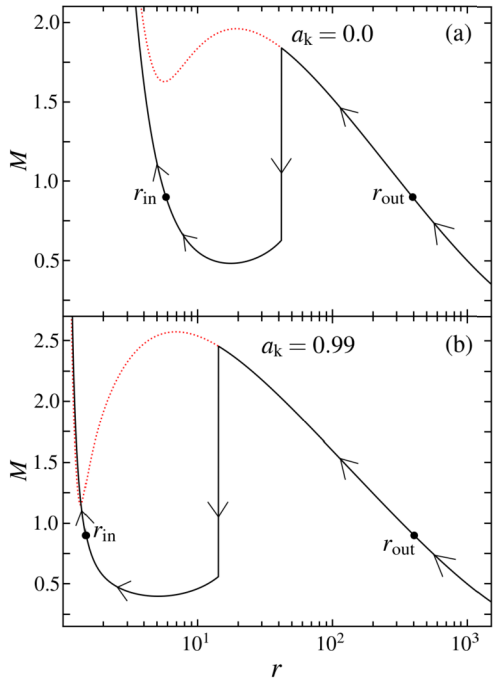

Fig. 3 Examples of shock-induced GTAS around a BH, where variations of M with r are depicted. The vertical down-arrow shows the shock transition radius, where Rankine–Hogoniot conditions (Landau and Lifshitz 1959) for a standing shock are satisfied. Filled circles denote critical points and arrows show the direction of the flow motion towards BH. The dotted curve represents the shock-free solution. (a) Upper panel is for $a_k = 0.0$, and (b) lower panel is for $a_k = 0.99$. See the text for details

ickam 2000; Das et al. 2009; Nagakura and Yamada 2009; Nandi et al. 2012; Iyer et al. 2015; Okuda and Das 2015; Suková and Janiuk 2015; Das et al. 2021). Accordingly, in the following sections, we investigate the shock-induced GTAS around BHs. In Fig. 2b, we present the variation of angular momentum for the solutions presented in Fig. 2a, where the big-dashed curve denotes the Keplerian angular momentum profile.

In Fig. 3a, we depict an example of a shock-induced global accretion solution, which passes thorough both $r_{out} = 395.32$ and $r_{in} = 5.808$ while accreting onto a stationary BH ($a_k = 0.0$). Here, matter is injected subsonically from $r_{edge} = 1500$ with $\lambda_{edge} = 4.68$, $\upsilon_{edge} = 8.35 \times 10^{-3}$, $\Theta_{edge} = 0.336$, $\dot{m} = 0.01$, $\alpha_0 = 0.01$, and $\theta = 0.1$. As subsonic matter proceeds towards the BH, it becomes supersonic at $r_{out} = 395.32$ and proceeds further towards the BH. Indeed, accreting matter can seamlessly cross the BH horizon after passing r_{out}, as shown by the dotted curve. Interestingly, supersonic accreting matter sees an alternate possibility of a discontinuous shock transition of the flow variables in the subsonic branch as the Rankine–Hogoniot conditions (RHCs) (Landau and Lifshitz 1959) for a standing shock are satisfied at the shock radius (r_s). We determine the standing shock location $r_s = 42.07$ for a vertically integrated flow by employing shock conditions (RHCs) that are (a) continuity of energy flux: $[\mathcal{E}] = 0$, (b) continuity of mass flux: $[\dot{M}] = 0$, and (c) continuity of momentum flux $[W + \Sigma\upsilon^2] = 0$ across the shock. Here, we express the local energy of the flow as $\mathcal{E} = \upsilon^2/2 + \log h + \Phi_e^{\rm eff}$, and the quantities within the bracket ([ ]) denote their differences across the shock-transition location. We show the shock transition using a vertical arrow. Immediately after the shock transition, the radial velocity of the matter decreases, however, it progressively increases as the matter proceeds towards the horizon. Eventually, matter crosses the BH horizon at supersonic speed after passing through the inner critical point at $r_{in} = 5.808$. In the figure, arrows show how the matter moves towards the BH. Note that the postshock branch of the shocked solution is similar in nature to the solution for $\theta = 0.3$ in Fig. 2. Further, we calculate the shock-induced GTAS around a rotating BH of $a_k = 0.99$ for flows injected with $\lambda_{edge} = 3.68$, $\upsilon_{edge} = 8.33 \times 10^{-3}$, $\Theta_{edge} = 0.342$, $\dot{m} = 0.01$, $\alpha_0 = 0.01$, and $\theta = 0.1$ from $r_{edge} = 1500$. The shock is formed at $r_s = 14.33$ in between $r_{out} = 405.46$ and $r_{in} = 1.492$. Here, we observe that for a chosen set of (α_0, θ), a shock exists around a rapidly rotating BH when λ_{edge} assumes a relatively smaller value and vice versa. Indeed, this is expected because accreting matter crosses the BH horizon with angular momentum lower than the marginally stable angular momentum (λ_{ms}) and λ_{ms} evidently decreases with the increase of a_k (Das and Chakrabarti 2008). In Table 2, we present the flow variables at the critical points for shock-induced GTAS presented in Fig. 3.

In Fig. 4, we present the profile of the different flow variables for the shocked accretion solution presented in Fig. 3. We depict the variation of the radial velocity (υ) in Fig. 4(a), where a discontinuous transition of υ is observed at the shock radius (r_s). We show the radial variation of mass density (ρ) of accreting matter in Fig. 4(b) and find that ρ increases monotonically with the decrease of r in the preshock branch, although a sudden jump of ρ is yielded across the shock front. Such a density jump at r_s is inevitable in order to maintain the conservation of mass flux (see equation (2)). Due to this, PSC experiences density compression that is eventually quantified in terms of the compression ratio defined as $R = \Sigma_+/\Sigma_-$, where Σ ($= 2\rho H$) is the vertically integrated mass density of the accretion flow at a given radial coordinate. We obtain $R = 2.31$. In Fig. 4(c), the variation of temperature (T in Kelvin) with r is shown. Indeed, the temperature of PSC shoots up as the kinetic energy of the upstream (preshock) flow is transformed into thermal energy in the downstream (postshock) flow, which eventually results in the increase of PSC temperature. Usually, the temperature jump at r_s is determined by means of the shock strength (S), and it is defined as $S = M_-/M_+$, where M_- (M_+) is the preshock (postshock) Mach number. We obtain $S = 2.92$. We present the entropy accretion

Table 2 Black-hole spin (a_k), critical-point location (r_c), angular momentum (λ_c), radial velocity (υ_c), and temperature (Θ_c) measured at r_c for the shocked accretion solution presented in Fig. 3. Subscript 'c' identifies quantities measured either at the inner ('in') or outer ('out') critical points. See text for more details

a_k	Critical Point	r_c (r_g)	λ_c ($r_g c$)	υ_c (c)	Θ_c ($m_e c^2 K$)
0	Inner	5.808	3.091	0.1794	27.4538
	Outer	395.32	3.470	0.0313	0.7580
0.99	Inner	1.492	2.058	0.2653	68.1666
	Outer	405.46	2.445	0.0312	0.7510

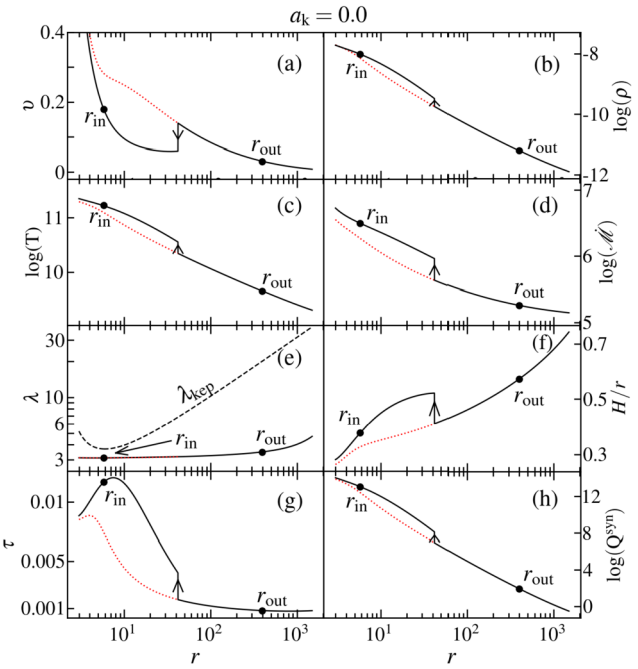

Fig. 4 Plot of (a) radial flow velocity υ, (b) density ρ, (c) Temperature T, (d) entropy accretion rate $\dot{\mathcal{M}}$, (e) angular momentum λ, (f) disk aspect ratio H/r, (g) optical depth τ, and (h) synchrotron emissivity Q^{syn} for a shocked accretion solution with r. Here, the vertical arrows indicate the shock-transition location. The dotted curve refers to a shock-free solution. See the text for details

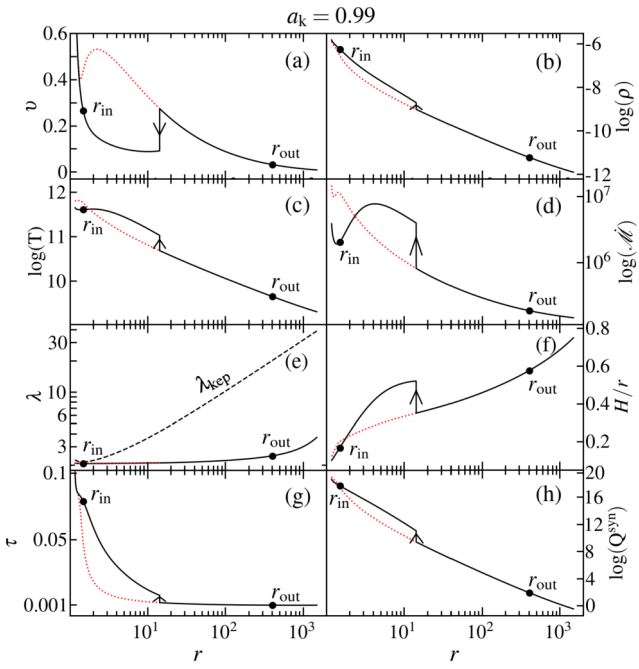

Fig. 5 Same as Fig. 4, but for flow accreting onto a rotating BH of $a_k = 0.99$

rate ($\dot{\mathcal{M}}$) in Fig. 4(d) and show that $\dot{\mathcal{M}}$ at PSC is larger compared to the preshock region. This discernibly indicates that the shock-induced GTAS are favorable over the shock-free GTAS according to the second law of thermodynamics (Becker and Kazanas 2001). We demonstrate the angular momentum (λ) variation in Fig. 4(e) and find that the transport of λ remains feeble within several hundred gravitational radii, although it increases rapidly towards the outer edge of the disk (r_{edge}). This possibly happens as the viscous time-scale becomes larger than the infall time-scale of accretion flow around BH. We show that the disc thickness scales with the radial coordinate in Fig. 4(f) and find that $H/r < 1$ is maintained throughout ($r_h \lesssim r \leq r_{edge}$) in the presence of a shock. Furthermore, we display the variation of scattering optical depth τ in Fig. 4g. In this work, τ is given by $\tau = \kappa\rho H$, where $\kappa = 0.38\ \mathrm{cm^2 g^{-1}}$. Since $\tau < 1$ particularly at $r < r_s$, the disc continues to remain optically thin there. Hence, the hard X-ray radiations originated from PSC would escape significantly with ease. In Fig. 4h, we present the synchrotron emissivity (in erg $\mathrm{cm^{-3}\ s^{-1}}$) with r. From the figure, it is evident that the net energy loss from PSC is high in comparison with the preshock flow.

In a similar way, we depict the different flow variables, such as υ, ρ, T, $\dot{\mathcal{M}}$, λ, H/r, τ, and Q^{syn} in Fig. 5 corresponding to the shocked accretion flow around a spinning BH of spin $a_k = 0.99$ presented in Figure 3b. The figure evidently indicates that the overall radial variations of these quantities are qualitatively similar with the results of $a_k = 0.0$, except in the region at the vicinity of the BH horizon (r_h). In particular, we find that τ continues to increase

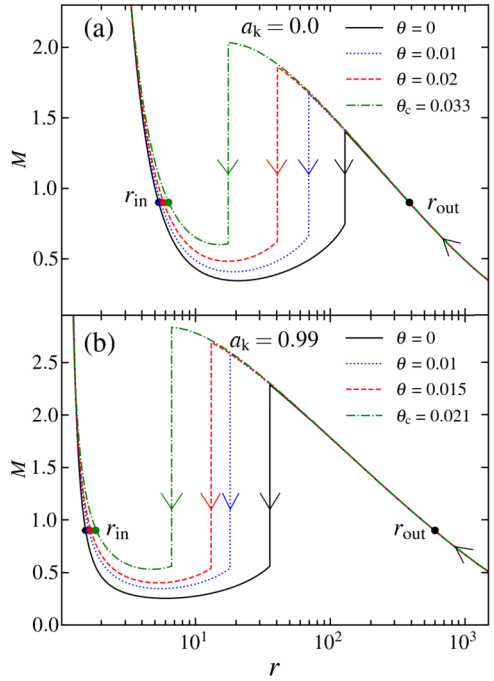

Fig. 6 Plot of M with r for accretion solutions that contain shock waves. Here, global parameters are chosen as $\dot{m} = 0.01$, and $\alpha_0 = 0.01$. *Top panel:* Flows with $\mathcal{E}_{\rm edge} = 1.0004$ and $\lambda_{\rm edge} = 4.01$ are injected from $r_{\rm edge} = 1500$ with different θ values onto a stationary BH of $a_{\rm k} = 0.0$. *Bottom panel:* Flows with $\mathcal{E}_{\rm edge} = 1.00023$ and $\lambda_{\rm edge} = 2.67$ at $r_{\rm edge} = 1500$ are injected with different θ values onto a rotating BH of $a_{\rm k} = 0.99$. Critical points are shown using filled circles and vertical down-arrows represent shock-transition radii. See the text for details

as the flow approaches the horizon ($r \to r_h$), although it is seen to decrease for a weakly rotating BH (see Fig. 4). This happens because τ is broadly regulated by the density (ρ) and ρ is increased significantly in the vicinity of a BH having $a_{\rm k} = 0.99$. We skip the detailed descriptions of other quantities to avoid repetitions.

In Fig. 6, we display how the shock radius changes with θ values for flows injected with fixed outer boundary values at $r_{\rm edge}$. Here, we choose $\dot{m} = 0.01$, and $\alpha_0 = 0.01$. In the top panel, we set the energy $\mathcal{E}_{\rm edge} = 1.0004$ and angular momentum $\lambda_{\rm edge} = 4.01$ at $r_{\rm edge} = 1500$ and allow the flow to accrete onto a nonrotating BH of $a_{\rm k} = 0.0$. We note that for $\theta = 0.0$, the subsonic flow becomes supersonic at $r_{\rm out} = 386.573$ and a shock is formed at $r_s = 129.30$ as the RH conditions are satisfied there. We also calculate the compression ratio as well as the shock strength for this solution and obtain these as $R = 1.65$ and $S = 1.88$. This solution is shown with a solid curve, whereas the solid vertical arrow denotes the shock radius. As θ is increased to $\theta = 0.01$, the shock front moves inwards at $r_s = 69.57$. This happens due to the fact that the increase of θ enhances the viscous effect in the accretion flow, and hence, the transport of λ in the outward direction becomes more intense. This effectively weakens the centrifugal repulsion causing the shock to move closer to the BH horizon. Evidently, this finding suggests that shock formation in the accretion flow is centrifugally driven. Here, we obtain $R = 2.07$ and $S = 2.51$. We plot this solution as a dotted curve. For the purpose of representation, we plot another solution for $\theta = 0.02$ using a dashed curve. Indeed, the value of θ cannot be increased indefinitely, and we find that beyond a limiting value of θ, which is $\theta_c = 0.033$, RHC for a shock are not favorable and hence, a shock does not form. Interestingly, a time-varying shock may still be possible, however, investigation of this is beyond the scope of this paper. Note that θ_c does not have a universal value as it is dependent on other flow variables. Accretion solutions for $\theta_c = 0.033$ are depicted using a dot-dashed curve. In the bottom panel, we present the shocked accretion solutions for flows accreting onto rotating BH of $a_{\rm k} = 0.99$. Here, we chose energy $\mathcal{E}_{\rm edge} = 1.00023$ and angular momentum $\lambda_{\rm edge} = 2.67$ at $r_{\rm edge} = 1500$. The solutions depicted with solid, dotted, dashed, and dot-dashed curves correspond to $\theta = 0$, 0.01, 0.015, and $\theta_c = 0.021$, respectively. In Table 3, we tabulate the flow quantities corresponding to these accretion solutions harboring shock waves.

In Fig. 7, variation of shock properties, namely shock radius r_s (upper panel), compression ratio R (middle panel), and shock strength S (lower) are depicted with θ. In the left panels, we display the results for the stationary BH of $a_{\rm k} = 0.0$, where flows are injected from $r_{\rm edge} = 1500$ with identical energy ($\mathcal{E}_{\rm edge} = 1.0004$) and angular momentum ($\lambda_{\rm edge} = 3.98$). Here, we set $\dot{m} = 0.01$ and obtain the results for $\alpha_0 = 0.01$ (solid), 0.011 (dashed), and 0.012 (dotted), respectively. Figure 7a clearly shows that stable shocks exist for an ample range of θ values. As already anticipated, for a fixed α_0, r_s decreases with θ as it weakens the centrifugal repulsion against the gravitational attraction. Moreover, for a given θ, when α_0 is higher, the angular-momentum transport becomes more efficient, weakening the centrifugal barrier. Due to this, the shock front proceeds inwards. Note that for a fixed α_0, when $\theta > \theta_c$, the shock disappears as RH conditions are not satisfied. As indicated earlier, θ_c strictly depends on the other flow variables (see Sect. 4). Indeed, the radiative cooling processes that primarily determine the flux of the high-energy radiations from the disk are strongly dependent on both ρ and T distributions across the shock front (Chakrabarti and Titarchuk 1995; Mandal and Chakrabarti 2005). Keeping this in mind, in Fig. 7b, we depict the variation of the compression ratio (R, measure of density compression across the shock) as a function of θ corresponding to shock-induced GTAS presented in Fig. 7a. We observe that when θ is increased, a shock is generally pushed towards the BH. Due to this, PSC becomes further compressed causing the overall increase of R. A similar trend is generally observed in the variation of R irrespective of the α_0 values provided a shock exists. Similarly, in Fig. 7c, we display

Table 3 Black-hole spin (a_k), power-law exponent (θ), inner critical-point location (r_{in}), inner critical-point angular momentum (λ_{in}), outer critical-point location (r_{out}), outer critical-point angular momentum (λ_{out}), shock radius (r_s), compression ratio (R), and shock strength (S) for global transonic solutions presented in Fig. 6. See text for more details

a_k	θ	r_{in} (r_g)	λ_{in} ($r_g c$)	r_{out} (r_g)	λ_{out} ($r_g c$)	r_s (r_g)	R	S
0	0	5.315	3.222	386.573	3.419	129.30	1.65	1.88
	0.01	5.520	3.162	387.529	3.373	69.57	2.07	2.51
	0.02	5.787	3.098	388.552	3.322	40.71	2.35	2.99
	0.033	6.295	3.007	389.986	3.252	17.58	2.54	3.35
0.99	0	1.529	2.122	601.228	2.368	35.78	2.90	4.10
	0.01	1.612	2.076	601.479	2.342	18.15	3.17	4.78
	0.015	1.668	2.052	601.615	2.329	13.13	3.24	4.99
	0.021	1.828	2.001	601.907	2.300	6.67	3.27	5.11

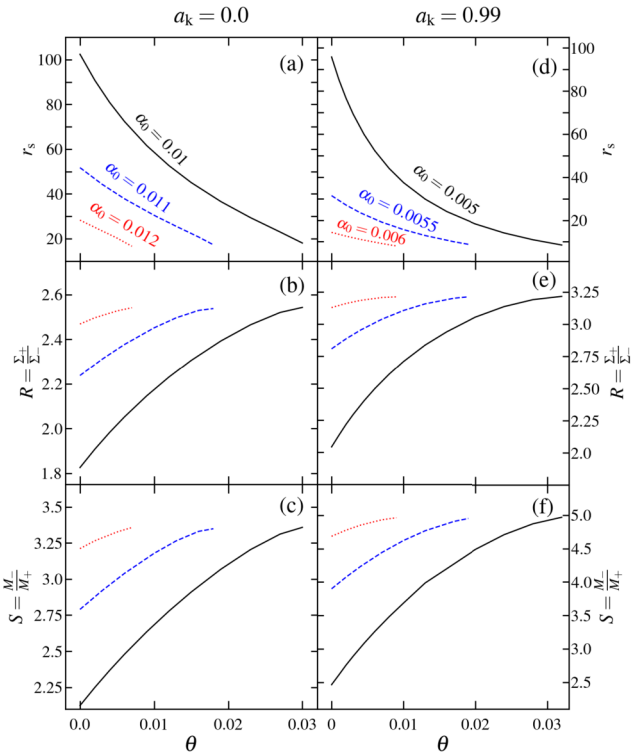

Fig. 7 Comparison of shock location r_s (upper panel), compression ratio R (middle panel), and shock strength S (lower panel) when varied with θ. Here, flows with the same energy and angular momentum are injected from the fixed outer edge (r_{edge}). *Left panels:* Results are obtained for $a_k = 0$, and solid, dashed, and dotted curves are drawn for $\alpha_0 = 0.01$, 0.011, and 0.012, respectively. *Right panels:* Results are for $a_k = 0.99$, where solid, dashed, and dotted curves correspond to $\alpha_0 = 0.005$, 0.0055, and 0.006, respectively. See the text for details

how shock strength (S, the measure of temperature jump across the shock front) varies with θ for the solutions presented in Fig. 7a. It is clear that for a fixed α_0, shock strength S monotonically increases as θ is increased and ultimately shifts from a weaker to a stronger regime. We continue the analyses and present the outcome for $a_k = 0.99$ in the right-hand panels of Fig. 7, where flows are injected from $r_{edge} = 1500$ with identical $\mathcal{E}_{edge} = 1.0004$, $\lambda_{edge} = 2.44$, and $\dot{m} = 0.001$. In order to preserve the θ range intact, here we chose a relatively smaller $\dot{m}$ compared to the same used for flows around weakly spinning BH. In Figs. 7d–f, results are obtained for $\alpha_0 = 0.005$ (solid), 0.0055 (dashed), and 0.006 (dotted), respectively. Note that the overall variations of r_s, R, and S with θ for $a_k = 0.99$ appear qualitatively similar, as delineated in the left panels for $a_k = 0.0$.

In Fig. 8, we investigate the effect of accretion rate ($\dot{m}$) for shock triggering in a convergent accretion flow. Such a portentous effort is very useful as the radiative cooling processes are regulated by $\dot{m}$. While doing so, we inject matter onto a nonrotating BH ($a_k = 0.0$) from $r_{edge} = 1500$ with $\mathcal{E}_{edge} = 1.0004$, $\lambda_{edge} = 3.98$ and $\alpha_0 = 0.01$. We display the obtained results in the left panels, where solid, dashed, and dotted curves correspond to $\dot{m} = 0.01$, 0.1, and 0.2, respectively. Similarly, for $a_k = 0.99$, we chose $r_{edge} = 1500$, $\mathcal{E}_{edge} = 1.0004$, $\lambda_{edge} = 2.44$, $\alpha_0 = 0.005$, and the results are drawn in the right panels. The spin values are marked at the top of the figure. In panels (a) and (d), we present the variation of r_s with θ, where shocks are seen to proceed further inward close to the BH horizon as θ increases. This feature is commonly observed irrespective of $\dot{m}$ values, provided a shock is formed. Furthermore, for a given θ, when $\dot{m}$ is increased, the shock front moves inward. This is not surprising because higher $\dot{m}$ eventually increases the effect of cooling in PSC, and accordingly, the thermal pressure decreases. Hence, the shock settles down at a location closer to the horizon to maintain the pressure balance on both sides of the discontinuity. In panels (b) and (e), we compare the compression ratio (R) and note that R increases with θ. This evidently indicates that for a convergent flow, accretion shock becomes stronger as r_s decreases. We further find that shock strength S increases monotonically with θ, and for a given

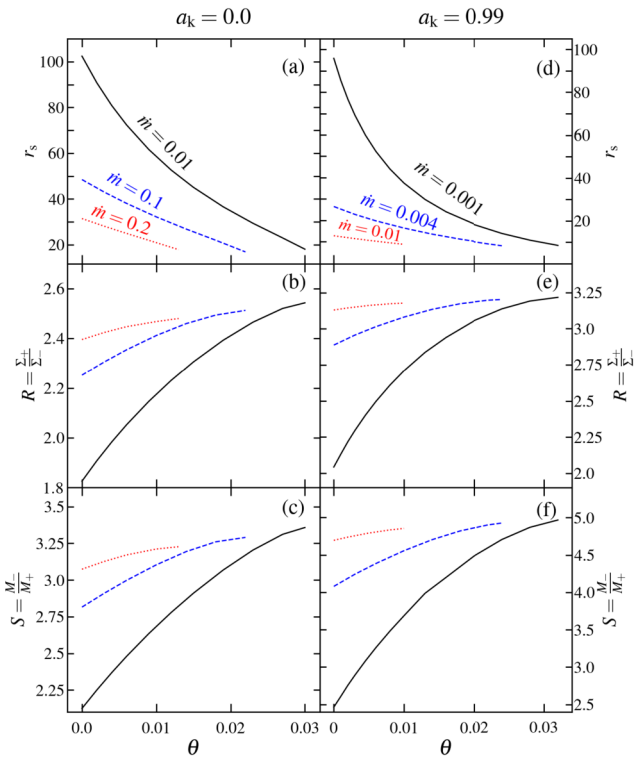

Fig. 8 Plot of r_s (upper panel), R (middle panel), and S (lower panel) with θ for flows with different $\dot{m}$. *Left panels:* Here, we choose $r_{\rm edge} = 1500$, $\mathcal{E}_{\rm edge} = 1.0004$, $\lambda_{\rm edge} = 3.98$, and $a_{\rm k} = 0.0$. Solid, dashed, and dotted curves are for $\dot{m} = 0.01$, 0.1, and 0.2. *Right panels:* We set $r_{\rm edge} = 1500$, $\mathcal{E}_{\rm edge} = 1.0004$, $\lambda_{\rm edge} = 2.44$, and $a_{\rm k} = 0.99$. Solid, dashed, and dotted curves are for $\dot{m} = 0.001$, 0.004, and 0.01. See the text for details

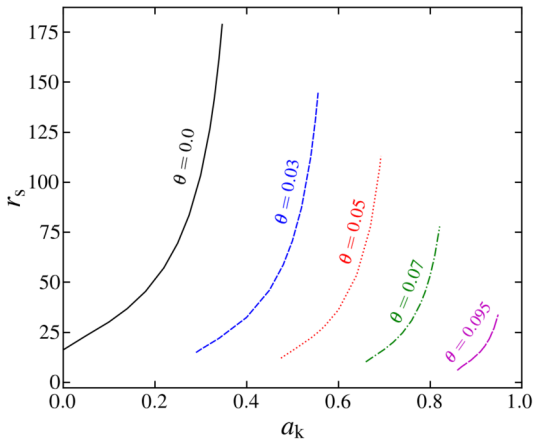

Fig. 9 Variation of r_s with $a_{\rm k}$ for different θ values. Results plotted using solid, dashed, dotted, dot-dashed, and big-dashed curves are for $\theta = 0.0, 0.03, 0.05, 0.07$, and 0.095. See the text for details

θ, when shocks form closer to BH, S is enhanced and vice versa (see panels (c) and (f)).

Next, we investigate the effect of BH rotation ($a_{\rm k}$) on r_s and present the obtained results in Fig. 9, where the variation of r_s with $a_{\rm k}$ for different θ is depicted. For this analysis, we inject matter from $r_{\rm edge} = 1500$ with $\lambda_{\rm edge} = 3.78$, $\mathcal{E}_{\rm edge} = 1.0004$, $\dot{m} = 0.01$, and $\alpha_0 = 0.01$. In the figure, solid, dashed, dotted, dot-dashed, and big-dashed curves are used to indicate results correspond to $\theta = 0.0, 0.03, 0.05, 0.07$, and 0.095, respectively. It is clear from the figure that for a fixed θ, r_s moves outwards from the BH horizon as θ increases for flows with fixed outer boundary conditions. Accordingly, the effective size of the PSC is increased, and hence, the possibility of upscattering the soft photons from the preshock disk at PSC is increased in producing the high-energy radiations. We further note that for a given θ, shocks form for a particular range of $a_{\rm k}$, and as θ is increased, the range of $a_{\rm k}$ is shifted to the higher side. This is not surprising because of the fact that for a fixed $\lambda_{\rm edge}$, higher θ increases angular-momentum transport causing the overall reduction of $\lambda(r)$ close to the BH. Indeed, it is evident that for higher $a_{\rm k}$, a shock exists when λ is relatively low (Das and Chakrabarti 2008), and this happens because of the spin-orbit coupling present in the effective potential (see equation (1a)) describing space–time geometry around the BH. These findings are consistent with the results of Sen et al. (2022). In contrast, we observe that r_s decreases due to the increase of θ for flows accreting onto a BH having a fixed spin ($a_{\rm k}$) value. Moreover, we observe that the lower limit of r_s is gradually reduced when the flow with a fixed outer boundary accretes onto the BHs of increasing spin ($a_{\rm k}$) values.

4 Shock-parameter space

In this section, we proceed further to identify the region of parameter space that admits stationary shock solutions for viscous advective accretion flow around BHs. It is evident from Figs. 6–9 that shock-induced GTAS are obtained for a range of angular momentum and θ values. Hence, we examine how the shock properties alter with θ in a viscous flow, and classify the effective domain of parameter space in terms of θ in the $\lambda_{\rm in} - \mathcal{E}_{\rm in}$ plane, where $\lambda_{\rm in}$ and $\mathcal{E}_{\rm in}$ refer to the angular momentum and energy of the flow at $r_{\rm in}$ (Aktar et al. 2017, 2019). We choose $\mathcal{E}_{\rm in}$ and $\lambda_{\rm in}$ in defining the shock-parameter space as the flow is expected to advect into the BH with energy and angular momentum resembling these values. The results are presented in Fig. 10, where the left panel is for $a_{\rm k} = 0.0$ and the effective region bounded with solid, dashed, dot-dashed, and dotted curves are for $\theta = 0.0, 0.1, 0.3$, and 0.35, respectively. Here, we set $\dot{m} = 0.01$. Similarly, in the bottom panel, we illustrate the results for $a_{\rm k} = 0.99$, where solid, dashed, dot-dashed, and dotted curves are used to separate the region for $\theta = 0.0, 0.3, 0.5$, and 0.7, respectively. Here, we choose $\dot{m} = 10^{-4}$. In each panel, $a_{\rm k}$ and θ values are marked. We observe that in both panels, the effective domain of $\lambda_{\rm in} - \mathcal{E}_{\rm in}$ space for a standing shock is reduced as θ increases. and accordingly, the

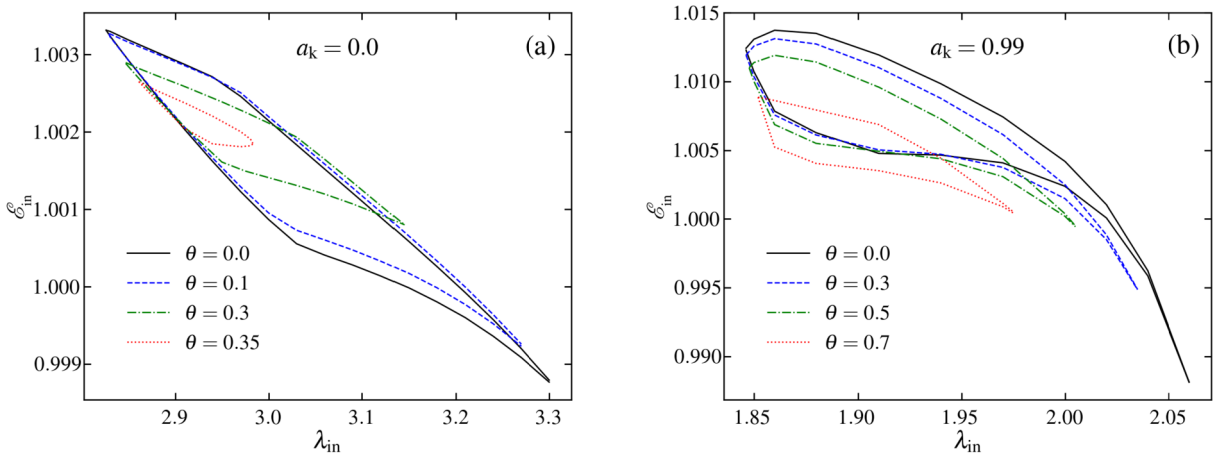

Fig. 10 Effective domain of the shock-parameter space as a function of θ. Upper panel (a) is for the stationary BH of $a_k = 0$, whereas bottom panel (b) illustrates results for the rapidly rotating BH of $a_k = 0.99$. See the text for details

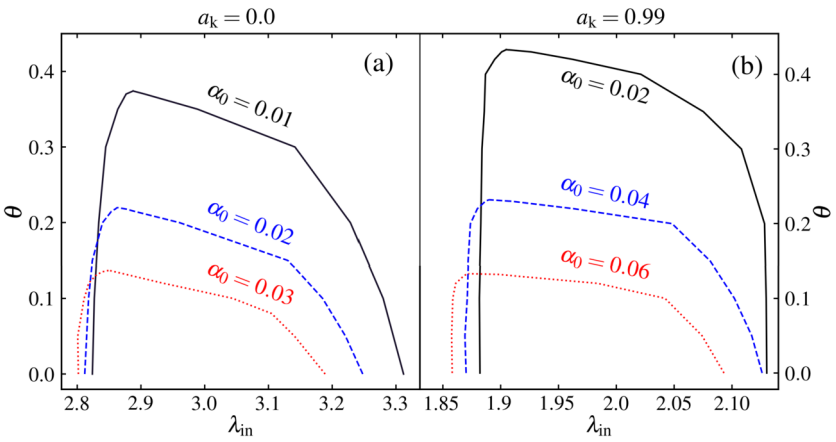

Fig. 11 Variation of θ with angular momentum at the inner critical point (λ_{in}) that admits a shock. In panel (a), $a_k = 0.0$ and solid, dashed, and dotted curves denote results for $\alpha_0 = 0.01$, 0.02, and 0.03, respectively. Similarly, in panel (b), $a_k = 0.99$, and solid, dashed, and dotted curves are for $\alpha_0 = 0.02$, 0.04, and 0.06. Here, we chose $\dot{m} = 0.01$. See the text for details

shock formation possibility is also diminished (Chakrabarti and Das 2004; Das 2007). Indeed, when θ exceeds its limiting value (*i.e.*, $\theta > \theta^{\max}$), the parameter space for a standing shock disappears. Note that for $\theta > \theta^{\max}$, the flow angular momentum in the vicinity of a BH is reduced to such an extent that the centrifugal barrier becomes very weak and it cannot trigger the shock transition. Hence, the standing shock ceases to exist. Nevertheless, time-dependent shocked accretion solutions may exist for $\theta > \theta^{\max}$, which were examined by numerical simulation to study the oscillatory behavior of shock solutions (Molteni et al. 1994; Das et al. 2014; Suková and Janiuk 2015; Lee et al. 2016). Interestingly, the solutions of this kind satisfactorily account for the quasiperiodic oscillations (QPOs) phenomena that are commonly observed in BH-XRBs (Nandi et al. 2012; Sreehari et al. 2020; Majumder et al. 2022). However, we indicate that the study of time-dependent shock solution is beyond the scope of this framework and we plan to consider it as future study.

We continue our study to examine the ranges of λ_{in} and θ in terms of α_0 that admit shocked-induced GTAS. In order to do that, we set $\dot{m} = 0.01$ and scan the range of θ for a given set of (λ_{in}, α_0) by freely varying r_{in} (equivalently $\mathcal{E}_{in}$). The obtained results for $a_k = 0.0$ and 0.99 are shown in Fig. 11. In panel (a), solid, dashed, and dotted curves are obtained for $\alpha_0 = 0.01$, 0.02, and 0.03, that separate the region for shocked accretion solutions from the shock-free solutions. Similarly, in panel (b), solid, dashed, and dotted curves are obtained for $\alpha_0 = 0.02$, 0.04, and 0.06. We observe that the permissible region for shock in $\lambda_{in} - \theta$ plane gradually diminishes with the increase of α_0 for both slowly and rapidly rotating BHs. In addition, we find that for a given α_0, θ attains its maximum value, namely $\theta^{\max}$, at a fixed λ_{in}. We further observe that as α_0 is increased, the value of $\theta^{\max}$ is decreased and it is obtained at smaller λ_{in} values.

In Fig. 12, we demonstrate how $\theta^{\max}$ varies with α_0. Open squares represent the results for $a_k = 0.0$, while open circles are for $a_k = 0.99$. These data points are further fitted empirically as $\theta^{\max} = \delta\alpha_0^{-1/2} - \eta e^{-\xi\alpha_0}$, where δ, η, and ξ are the constants, and their values strictly depend on a_k, which are presented in Table 4. In the figure, solid curves denote the best-fit representations of the fitted func-

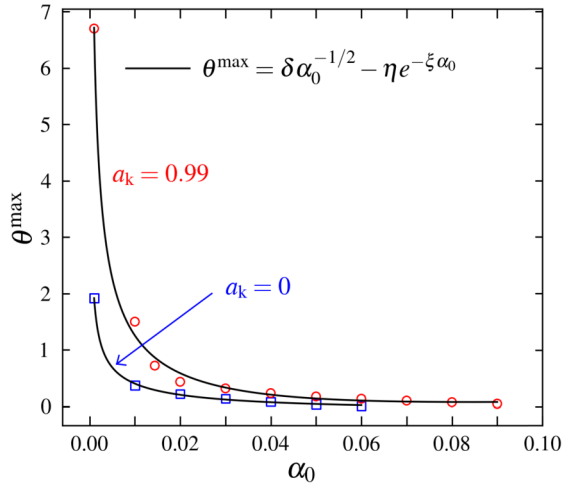

Fig. 12 Plot of $\theta^{\max}$ as a function of α_0 for shocked accretion solutions. Results depicted using open squares and open circles are for $a_k = 0.0$ and 0.99, respectively. Solid curves denote the fitted function as mentioned in the text. Here, we choose $\dot{m} = 0.01$. See the text for details

Table 4 Values of the coefficients obtained from the best-fit representation of $\theta^{\max}$ $(= \delta\alpha_0^{-1/2} - \eta e^{-\xi\alpha_0})$ yielding shock-induced GTAS (see Fig. 12). See the text for details

a_k	δ	η	ξ
0	0.07	0.31	2.50
0.99	0.25	1.39	6.48

tion described above for $a_k = 0.0$ and 0.99, respectively. Figure 12 clearly indicates that the accretion flows with relatively higher viscosity continue to harbor shock waves around the highly spinning BHs as compared to the weakly rotating BHs. This happens mostly because the outer critical points turn into nodal types (Dihingia et al. 2019b) at higher viscosity for $a_k \to 0$, and hence, shock-induced GTAS ceases to exist.

5 Conclusions

In this study, we examine the structure of the viscous accretion flow that includes the more general viscosity than those usually discussed in the literature (Narayan and Yi 1994; Chakrabarti 1996; Chakrabarti and Das 2004, and references therein). In particular, we consider the viscosity parameter to vary with the radial coordinate as $\alpha(r)$ and observe that GTAS continue to exist around a rotating BH. Depending on input parameters, *i.e.*, viscosity, angular momentum, accretion rate, the accretion flow may harbor shock waves. Indeed, the shock-induced GTAS is promising in the sense that it has the potential to explain the spectrotemporal properties of BH sources (Chakrabarti and Manickam 2000; Nandi et al. 2001; Smith et al. 2001, 2002; Nandi et al. 2012; Iyer et al. 2015; Das et al. 2021). We find important results that are presented below.

1. There exist global transonic accretion solutions that either pass through inner critical points ($r_{\rm in}$, ADAF-type) or outer critical points ($r_{\rm out}$, Bondi-type) for low angular momentum flow. We find that when viscosity is appropriately chosen by tuning the viscosity exponent θ, keeping the other flow parameter fixed at the outer edge ($r_{\rm edge}$), ADAF-type solutions change their character to become Bondi-type (see Fig. 1). Further, when θ is decreased for an ADAF-type solution, the global accretion solution eventually becomes closed as it could not extend up to the disk outer edge (see Fig. 2), although it can join with a Bondi-type solution via a Rankine–Hugoniot shock transition (see Fig. 3). Note that these findings are seen in both weakly rotating ($a_k \to 0$) and rapidly rotating ($a_k \to 1$) BHs. Since it is generally perceived that BHs may accrete low angular momentum matter from their surroundings stars, shock seems to be an indispensable component in the accretion flow.
2. We observe that because of shock transition, convergent accretion flow is compressed, yielding hot and dense PSC (see Figs. 4 and 5). Thus, PSC contains a swarm of hot electrons, which are likely to reprocess the low-energy photons from preshock flow via inverse-Comptonization and generate hard X-ray radiations (Chakrabarti and Titarchuk 1995; Mandal and Chakrabarti 2005). Such a signature of excess high-energy radiations is often observed from galactic X-ray binaries harboring BH sources (Sunyaev and Titarchuk 1980; Iyer et al. 2015; Baby et al. 2020, and references therein). With this, we infer that the shock radius (r_s), which coarsely measures the size of PSC, seems to play a viable role to emit hard X-ray radiations from the accretion disc.
3. When viscosity is enhanced, the efficiency of the angular momentum transport increases that evidently weakens the centrifugal repulsion against gravity. Due to this, for higher θ, the size of PSC is reduced as the shock front moves inward to satisfy the pressure equilibrium on both sides of the discontinuity (see Fig. 6). Accordingly, by suitably changing θ, one can regulate the accreting dynamics including PSC while explaining the disk emission.
4. We determine the limiting range of flow parameters that admit a shock transition in viscous accretion flow around both slowly and rapidly rotating BHs. We find that shock-induced GTAS are not discrete solutions. In fact, solutions of this kind are obtained for an ample range of flow parameters (see Fig. 10). However, the possibility of shock formation diminishes as we increase viscosity, and beyond a critical limit of $\theta > \theta^{\max}$, shocks disappear.

Indeed, $\theta^{\max}$ does not have a universal value as it is dependent on other flow variables.

5. We quantify $\theta^{\max}$ as a function of α_0 for $a_k = 0$ and 0.99, and find that it sharply decreases at lower α_0 and ultimately settles down to its asymptotic limit (see Fig. 12).

It is noteworthy that in the literature, there exist results of shock-induced transonic accretion flows obtained from simulation studies (Chakrabarti and Molteni 1995; Lanzafame et al. 1998; Giri and Chakrabarti 2012; Das et al. 2014; Okuda and Das 2015; Lee et al. 2016). Indeed, in all these works, the viscosity parameter (α) was treated as a global constant throughout the disk. On the contrary, adopting the variable viscosity prescription, numerical simulation results of accretion flows around BHs are also reported. In particular, Hawley and Krolik (2001, 2002) examined the dynamical behavior of the azimuthally and time-averaged α that typically ranges between ~ 0.01 and ~ 0.1 throughout most of the disk. Penna et al. (2013) reported a feeble variation of α ($\sim 0.01 - 0.3$) across the disk length scale with a peak around $2 - 3r_g$. In studying a truncated accretion disk, Hogg and Reynolds (2018) obtained $\alpha \sim 0.07$ at $\sim 600r_g$ in the quasisteady state, although α settles down to ≈ 0.02 at the inner edge of the disk. Evidently, in these variable-α studies, the formation of shock is not observed simply because these simulations were performed with Keplerian or quasi-Keplerian flows that are subsonic in nature and hence, are incapable of triggering a shock transition (Das et al. 2001). Accordingly, it remains infeasible to compare the results obtained from the present formalism with the existing simulations. Nevertheless, we infer that with the suitable choices of the input parameters, accretion flow having variable α would possibly be capable of possessing a shock, as corroborated in Giri and Chakrabarti (2013). We further indicate that based on the above findings, the quantitative description of the viscosity profile adopted in the present formalism seems to be fairly consistent with the results of the simulation works.

We further mention that in an accreting system, PSC seems to play a vital role in deciphering the observational signatures commonly observed in BH X-ray binary sources. As indicated earlier, PSC can reprocess the soft photons via inverse Comptonization to produce hard X-ray radiations that eventually contribute in generating the high-energy tail of the energy spectrum (Chakrabarti and Titarchuk 1995; Mandal and Chakrabarti 2005). Occasionally, Galactic X-ray binaries do show spectral state transitions, which possibly resulted when PSC geometry changes (Nandi et al. 2012; Iyer et al. 2015, and references therein). When PSC demonstrates time-varying modulation, it resembles an astonishing phenomenon known as Quasiperiodic Oscillations (QPO) of hard X-ray radiations (Chakrabarti and Manickam 2000; Nandi et al. 2001; Das et al. 2014). Moreover, it has been reported that PSC can deflect a part of the accreting matter in the form of jets/outflow (Das et al. 2001b, 2014; Aktar et al. 2017, 2018; Nandi et al. 2018). Considering all these, we argue that the present formalism in examining the PSC characteristics is strongly relevant in the astrophysical context.

Finally, we indicate the limitations of this formalism as it is developed considering several assumptions. We use an effective potential to describe the space–time geometry around the rotating BH avoiding a rigorous general-relativistic approach. We neglect structured large-scale magnetic fields and use a stochastic magnetic-field configuration. We also consider the flow to remain confined in a single-temperature domain although flow is expected to maintain two-temperature (for both ions and electrons) profiles. Implementation of all such issues is beyond the scope of this work and we intend to take up these relevant issues in future projects.

Detailed expression of the wind equation

With some simple algebraic steps, the radial momentum equations, azimuthal momentum equations, and entropy generation equations are reduced to the following form as:

$$R_0 + R_\upsilon \frac{d\upsilon}{dr} + R_\Theta \frac{d\Theta}{dr} + R_\lambda \frac{d\lambda}{dr} = 0, \tag{A1}$$

$$L_0 + L_\upsilon \frac{d\upsilon}{dr} + L_\Theta \frac{d\Theta}{dr} + L_\lambda \frac{d\lambda}{dr} = 0, \tag{A2}$$

$$E_0 + E_\upsilon \frac{d\upsilon}{dr} + E_\Theta \frac{d\Theta}{dr} + E_\lambda \frac{d\lambda}{dr} = 0. \tag{A3}$$

Using equations (A1–A3), we obtain the wind equation, the derivative of angular momentum, and the derivative of temperature, which are given by:

$$\frac{d\upsilon}{dr} = \frac{\mathcal{N}}{\mathcal{D}}, \tag{A4}$$

$$\frac{d\lambda}{dr} = \lambda_1 + \lambda_2 \frac{d\upsilon}{dr}, \tag{A5}$$

$$\frac{d\Theta}{dr} = \Theta_1 + \Theta_2 \frac{d\upsilon}{dr}, \tag{A6}$$

where,

$$\mathcal{N} = E_\lambda \left(-R_\Theta L_0 + R_0 L_\Theta\right) + E_\Theta \left(R_\lambda L_0 - R_0 L_\lambda\right) + E_0 \left(-R_\lambda L_\Theta + R_\Theta L_\lambda\right),$$

$$\mathcal{D} = E_\lambda \left(R_\Theta L_\upsilon + R_\upsilon L_\Theta\right) + E_\Theta \left(-R_\lambda L_\upsilon + R_\upsilon L_\lambda\right) + E_\upsilon \left(R_\lambda L_\Theta - R_\Theta L_\lambda\right),$$

$$\Theta_1 = \frac{\Theta_{11}}{\Theta_{33}} \quad \Theta_2 = \frac{\Theta_{22}}{\Theta_{33}}, \quad \lambda_1 = \frac{\lambda_{11}}{\Theta_{33}}, \quad \lambda_2 = \frac{\lambda_{22}}{\Theta_{33}},$$

$$\Theta_{11} = E_\lambda L_0 - E_0 L_\lambda, \quad \Theta_{22} = E_\lambda L_\upsilon - E_\upsilon L_\lambda,$$

$$\Theta_{33} = -E_\lambda L_\Theta + E_\Theta L_\lambda,$$

$$\lambda_{11} = -E_\Theta L_0 + E_0 L_\Theta, \quad \lambda_{22} = -E_\Theta L_\upsilon + E_\upsilon L_\Theta,$$

$$R_0 = \frac{d\Phi_e^{\rm eff}}{dr} - \frac{3\Theta}{r\tau h} + \frac{F_1\Theta}{\tau\mathcal{F}h} - \frac{\Theta\Delta'}{\tau\Delta h},$$

$$R_\Theta = \frac{1}{\tau h}, \tau = 1 + \frac{m_p}{m_e},$$

$$R_\lambda = \frac{F_2\Theta}{\tau\mathcal{F}h}, \; R_\upsilon = \upsilon - \frac{2\Theta}{\tau\upsilon h}, \; \Delta' = \frac{d\Delta}{dr},$$

$$E_0 = -\frac{Q^-}{\rho} - r\alpha\upsilon^2\omega_1 - \frac{2r\alpha\Theta\omega_1}{\tau} + \frac{\upsilon\Theta\left(-rF_1\Delta + \mathcal{F}(3\Delta + r\Delta')\right)}{r\tau\Delta},$$

$$E_\Theta = \frac{(1+2n\upsilon)}{\tau}, \; E_\lambda - \frac{\left(F_2\upsilon\Theta + r\alpha\mathcal{F}(\tau\upsilon^2 + 2\Theta)\omega_2\right)}{\tau\mathcal{F}},$$

$$E_\upsilon = \frac{2\theta}{\tau},$$

$$L_0 = -2\alpha\upsilon^2 - \frac{4\alpha\Theta}{\tau} + \frac{r\alpha\upsilon^2\Delta'}{2\Delta} + \frac{r\alpha\Theta\Delta'}{\tau\Delta} - \frac{r}{\tau}\left(\tau\upsilon^2 + 2\Theta\right)\frac{d\alpha}{dr},$$

$$L_\Theta = -\frac{2r\alpha}{\tau}, \; L_\lambda = \upsilon, \; L_\upsilon = -r\alpha\upsilon + \frac{2r\alpha\Theta}{\tau\upsilon},$$

$$F_1 = \frac{F\lambda\omega_1}{(1-\lambda\Omega)^2} + \frac{1}{1-\lambda\Omega}\frac{dF}{dr},$$

$$F_2 = \frac{F\Omega}{(1-\lambda\Omega)^2} + \frac{F\lambda\omega_2}{(1-\lambda\Omega)^2}, \; \mathcal{F} = \frac{1}{(1-\lambda\Omega)}F,$$

$$F = \frac{(r^2+a_{\rm k}^2)^2 + 2\Delta a_{\rm k}^2}{(r^2+a_{\rm k}^2)^2 - 2\Delta a_{\rm k}^2}, \; \frac{d\mathcal{F}}{dr} = F_1 + F_2\frac{d\lambda}{dr},$$

$$\frac{d\Omega}{dr} = \omega_1 + \omega_2\frac{d\lambda}{dr},$$

$$\omega_1 = -\frac{2\left(a_{\rm k}^3 + 3a_{\rm k}r^2 + \lambda(a_{\rm k}\lambda - 2a_{\rm k}^2 + r^2(r-3))\right)}{\left(r^3 + a_{\rm k}^2(r+2) - 2a_{\rm k}\lambda\right)^2},$$

$$\omega_2 = \frac{r^2\left(a_{\rm k}^2 + r(r-2)\right)}{\left(r^3 + a_{\rm k}^2(r+2) - 2a_{\rm k}\lambda\right)^2}.$$

Acknowledgements This work was supported by the Science and Engineering Research Board (SERB) of India through grant MTR/2020/000331.

Author contributions MS generated results and prepared all figures. SD wrote the main manuscript text. All authors reviewed the manuscript.

Data Availability The data underlying this article will be available upon reasonable request.

Declarations

Competing interests The authors declare no competing interests.

References

Abramowicz, M.A., Chakrabarti, S.K.: Standing shocks in adiabatic black hole accretion of rotating matter. Astrophys. J. **350**, 281 (1990). https://doi.org/10.1086/168380

Aktar, R., Das, S., Nandi, A., et al.: Estimation of mass outflow rates from dissipative accretion disc around rotating black holes. Mon. Not. R. Astron. Soc. **471**(4), 4806–4819 (2017). https://doi.org/10.1093/mnras/stx1893. arXiv:1707.07511 [astro-ph.HE]

Aktar, R., Das, S., Nandi, A., et al.: Advective accretion flow properties around rotating black holes – application to GRO J1655-40. J. Astrophys. Astron. **39**(1), 17 (2018). https://doi.org/10.1007/s12036-017-9507-0. arXiv:1801.04116 [astro-ph.HE]

Aktar, R., Nandi, A., Das, S.: Accretion-ejection in rotating black holes: a model for 'outliers' track of radio-X-ray correlation in X-ray binaries. Astrophys. Space Sci. **364**(2), 22 (2019). https://doi.org/10.1007/s10509-019-3509-0. arXiv:1901.10091 [astro-ph.HE]

Baby, B.E., Agrawal, V.K., Ramadevi, M.C., et al.: AstroSat and MAXI view of the black hole binary 4U 1630-472 during 2016 and 2018 outbursts. Mon. Not. R. Astron. Soc. **497**(1), 1197–1211 (2020). https://doi.org/10.1093/mnras/staa1965. arXiv:2007.00928 [astro-ph.HE]

Balbus, S.A., Hawley, J.F.: A powerful local shear instability in weakly magnetized disks. I. Linear analysis. Astrophys. J. **376**, 214 (1991). https://doi.org/10.1086/170270

Balbus, S.A., Hawley, J.F.: Instability, turbulence, and enhanced transport in accretion disks. Rev. Mod. Phys. **70**(1), 1–53 (1998). https://doi.org/10.1103/RevModPhys.70.1

Becker, P.A., Kazanas, D.: Exact expressions for the critical Mach numbers in the two-fluid model of cosmic-ray-modified shocks. Astrophys. J. **546**(1), 429–446 (2001). https://doi.org/10.1086/318257. arXiv:astro-ph/0101020 [astro-ph]

Bondi, H.: On spherically symmetrical accretion. Mon. Not. R. Astron. Soc. **112**, 195 (1952). https://doi.org/10.1093/mnras/112.2.195

Chakrabarti, S.K.: Standing Rankine-Hugoniot shocks in the hybrid model flows of the black hole accretion and winds. Astrophys. J. **347**, 365 (1989). https://doi.org/10.1086/168125

Chakrabarti, S.K.: Grand unification of solutions of accretion and winds around black holes and neutron stars. Astrophys. J. **464**, 664 (1996). https://doi.org/10.1086/177354. arXiv:astro-ph/9606145 [astro-ph]

Chakrabarti, S.K., Das, S.: Properties of accretion shock waves in viscous flows around black holes. Mon. Not. R. Astron. Soc. **349**(2), 649–664 (2004). https://doi.org/10.1111/j.1365-2966.2004.07536.x. arXiv:astro-ph/0402561 [astro-ph]

Chakrabarti, S.K., Manickam, S.G.: Correlation among quasi-periodic oscillation frequencies and quiescent-state duration in black hole candidate GRS 1915 + 105. Astrophys. J. Lett. **531**(1), L41–L44 (2000). https://doi.org/10.1086/312512. arXiv:astro-ph/9910012 [astro-ph]

Chakrabarti, S.K., Molteni, D.: Viscosity prescriptions in accretion discs with shock waves. Mon. Not. R. Astron. Soc. **272**(1), 80–88 (1995). https://doi.org/10.1093/mnras/272.1.80

Chakrabarti, S., Titarchuk, L.G.: Spectral properties of accretion disks around galactic and extragalactic black holes. Astrophys. J. **455**, 623 (1995). https://doi.org/10.1086/176610. arXiv:astro-ph/9510005 [astro-ph]

Chattopadhyay, I., Chakrabarti, S.K.: A comparative study of bondi-type and radiative outflows around compact objects. Int. J. Mod. Phys. D **9**(6), 717–731 (2000). https://doi.org/10.1142/S0218271800000670

Chattopadhyay, I., Kumar, R.: Estimation of mass outflow rates from viscous relativistic accretion discs around black holes. Mon. Not. R. Astron. Soc. **459**(4), 3792–3811 (2016). https://doi.org/10.1093/mnras/stw876. arXiv:1605.00752 [astro-ph.HE]

Chattopadhyay, I., Ryu, D.: Effects of fluid composition on spherical flows around black holes. Astrophys. J. **694**(1), 492–501 (2009). https://doi.org/10.1088/0004-637X/694/1/492. arXiv:0812.2607 [astro-ph]

Das, S.: Behaviour of dissipative accretion flows around black holes. Mon. Not. R. Astron. Soc. **376**(4), 1659–1670 (2007). https://doi.org/10.1111/j.1365-2966.2007.11501.x. arXiv:astro-ph/0610651 [astro-ph]

Das, S., Chakrabarti, S.K.: Dissipative accretion flows around a rotating black hole. Mon. Not. R. Astron. Soc. **389**(1), 371–378 (2008). https://doi.org/10.1111/j.1365-2966.2008.13564.x. arXiv:0806.1985 [astro-ph]

Das, S., Sarkar, B.: Standing shocks in magnetized advection accretion flows onto a rotating black hole. Mon. Not. R. Astron. Soc. **480**(3), 3446–3456 (2018). https://doi.org/10.1093/mnras/sty2071. arXiv:1807.11417 [astro-ph.HE]

Das, S., Chattopadhyay, I., Chakrabarti, S.K.: Standing shocks around black holes: an analytical study. Astrophys. J. **557**(2), 983–989 (2001). https://doi.org/10.1086/321692. arXiv:astro-ph/0107046 [astro-ph]

Das, S., Chattopadhyay, I., Nandi, A., et al.: Computation of outflow rates from accretion disks around black holes. Astron. Astrophys. **379**, 683–689 (2001b). https://doi.org/10.1051/0004-6361:20011307. arXiv:astro-ph/0402555 [astro-ph]

Das, S., Becker, P.A., Le, T.: Dynamical structure of viscous accretion disks with shocks. Astrophys. J. **702**(1), 649–659 (2009). https://doi.org/10.1088/0004-637X/702/1/649. arXiv:0907.0875 [astro-ph.HE]

Das, S., Chattopadhyay, I., Nandi, A., et al.: Periodic mass loss from viscous accretion flows around black holes. Mon. Not. R. Astron. Soc. **442**(1), 251–258 (2014). https://doi.org/10.1093/mnras/stu864. arXiv:1405.4415 [astro-ph.HE]

Das, S., Nandi, A., Agrawal, V.K., et al.: Relativistic viscous accretion flow model for ULX sources: a case study for IC 342 X-1. Mon. Not. R. Astron. Soc. **507**(2), 2777–2781 (2021). https://doi.org/10.1093/mnras/stab2307. arXiv:2108.02973 [astro-ph.HE]

Dihingia, I.K., Das, S., Maity, D., et al.: Limitations of the pseudo-Newtonian approach in studying the accretion flow around a Kerr black hole. Phys. Rev. D **98**, 083,004 (2018). https://doi.org/10.1103/PhysRevD.98.083004

Dihingia, I.K., Das, S., Maity, D., et al.: Shocks in relativistic viscous accretion flows around Kerr black holes. Mon. Not. R. Astron. Soc. **488**(2), 2412–2422 (2019a). https://doi.org/10.1093/mnras/stz1933. arXiv:1903.02856 [astro-ph.HE]

Dihingia, I.K., Das, S., Nandi, A.: Low angular momentum relativistic hot accretion flow around Kerr black holes with variable adiabatic index. Mon. Not. R. Astron. Soc. **484**(3), 3209–3218 (2019b). https://doi.org/10.1093/mnras/stz168. arXiv:1901.04293 [astro-ph.HE]

Fragile, P.C., Blaes, O.M., Anninos, P., et al.: Global general relativistic magnetohydrodynamic simulation of a tilted black hole accretion disk. Astrophys. J. **668**(1), 417–429 (2007). https://doi.org/10.1086/521092. arXiv:0706.4303 [astro-ph]

Fukue, J.: Transonic disk accretion revisited. Publ. Astron. Soc. Jpn. **39**(2), 309–327 (1987)

Giri, K., Chakrabarti, S.K.: Hydrodynamic simulations of viscous accretion flows around black holes. Mon. Not. R. Astron. Soc. **421**(1), 666–678 (2012). https://doi.org/10.1111/j.1365-2966.2011.20343.x. arXiv:1112.1500 [astro-ph.HE]

Giri, K., Chakrabarti, S.K.: Hydrodynamic simulation of two-component advective flows around black holes. Mon. Not. R. Astron. Soc. **430**(4), 2836–2843 (2013). https://doi.org/10.1093/mnras/stt087. arXiv:1212.6493 [astro-ph.HE]

Hawley, J.F., Krolik, J.H.: Global MHD simulation of the inner accretion disk in a pseudo-Newtonian potential. Astrophys. J. **548**(1), 348–367 (2001). https://doi.org/10.1086/318678. arXiv:astro-ph/0006456 [astro-ph]

Hawley, J.F., Krolik, J.H.: High-resolution simulations of the plunging region in a pseudo-Newtonian potential: dependence on numerical resolution and field topology. Astrophys. J. **566**(1), 164–180 (2002). https://doi.org/10.1086/338059. arXiv:astro-ph/0110118 [astro-ph]

Hawley, J.F., Gammie, C.F., Balbus, S.A.: Local three-dimensional magnetohydrodynamic simulations of accretion disks. Astrophys. J. **440**, 742 (1995). https://doi.org/10.1086/175311

Hawley, J.F., Gammie, C.F., Balbus, S.A.: Local three-dimensional simulations of an accretion disk hydromagnetic dynamo. Astrophys. J. **464**, 690 (1996). https://doi.org/10.1086/177356

Hogg, J.D., Reynolds, C.S.: The dynamics of truncated black hole accretion disks. II. Magnetohydrodynamic case. Astrophys. J. **854**(1), 6 (2018). https://doi.org/10.3847/1538-4357/aaa6c6. arXiv:1801.05836 [astro-ph.HE]

Iyer, N., Nandi, A., Mandal, S.: Determination of the mass of IGR J17091-3624 from "spectro-temporal" variations during the onset phase of the 2011 outburst. Astrophys. J. **807**(1), 108 (2015). https://doi.org/10.1088/0004-637X/807/1/108. arXiv:1505.02529 [astro-ph.HE]

King, A.R., Pringle, J.E., Livio, M.: Accretion disc viscosity: how big is alpha? Mon. Not. R. Astron. Soc. **376**(4), 1740–1746 (2007). https://doi.org/10.1111/j.1365-2966.2007.11556.x. arXiv:astro-ph/0701803 [astro-ph]

Kumar, R., Chattopadhyay, I.: Dissipative advective accretion disc solutions with variable adiabatic index around black holes. Mon. Not. R. Astron. Soc. **443**(4), 3444–3462 (2014). https://doi.org/10.1093/mnras/stu1389. arXiv:1407.2130 [astro-ph.HE]

Landau, L.D., Lifshitz, E.M.: Fluid Mechanics. Pergamon Press, Oxford (1959)

Lanzafame, G., Molteni, D., Chakrabarti, S.K.: Smoothed particle hydrodynamic simulations of viscous accretion discs around black holes. Mon. Not. R. Astron. Soc. **299**(3), 799–804 (1998). https://doi.org/10.1046/j.1365-8711.1998.01816.x. arXiv:astro-ph/9706248 [astro-ph]

Lee, S.J., Chattopadhyay, I., Kumar, R., et al.: Simulations of viscous accretion flow around black holes in a two-dimensional cylindrical geometry. Astrophys. J. **831**(1), 33 (2016). https://doi.org/10.3847/0004-637X/831/1/33. arXiv:1608.03997 [astro-ph.HE]

Lu, J.F., Gu, W.M., Yuan, F.: Global dynamics of advection-dominated accretion revisited. Astrophys. J. **523**(1), 340–349 (1999). https://doi.org/10.1086/307725. arXiv:astro-ph/9905099 [astro-ph]

Lyubarskii, Y.E.: Flicker noise in accretion discs. Mon. Not. R. Astron. Soc. **292**(3), 679–685 (1997). https://doi.org/10.1093/mnras/292.3.679

Majumder, S., Sreehari, H., Aftab, N., et al.: Wide-band view of high-frequency quasi-periodic oscillations of GRS 1915 + 105 in 'softer' variability classes observed with AstroSat. Mon. Not. R. Astron. Soc. **512**(2), 2508–2524 (2022). https://doi.org/10.1093/mnras/stac615. arXiv:2203.02710 [astro-ph.HE]

Mandal, S., Chakrabarti, S.K.: Accretion shock signatures in the spectrum of two-temperature advective flows around black holes. Astron. Astrophys. **434**(3), 839–848 (2005). https://doi.org/10.1051/0004-6361:20041235

Matsumoto, R., Tajima, T.: Magnetic viscosity by localized shear flow instability in magnetized accretion disks. Astrophys. J. **445**, 767 (1995). https://doi.org/10.1086/175739

Matsumoto, R., Kato, S., Fukue, J., et al.: Viscous transonic flow around the inner edge of geometrically thin accretion disks. Publ. Astron. Soc. Jpn. **36**(1), 71–85 (1984)

Mitra, S., Maity, D., Dihingia, I.K., et al.: Study of general relativistic magnetohydrodynamic accretion flow around black holes. Mon. Not. R. Astron. Soc. **516**(4), 5092–5109 (2022). https://doi.org/10.1093/mnras/stac2431. arXiv:2204.01412 [astro-ph.HE]

Molteni, D., Lanzafame, G., Chakrabarti, S.K.: Simulation of thick accretion disks with standing shocks by smoothed particle hydrodynamics. Astrophys. J. **425**, 161 (1994). https://doi.org/10.1086/173972. arXiv:astro-ph/9310047 [astro-ph]

Molteni, D., Sponholz, H., Chakrabarti, S.K.: Resonance oscillation of radiative shock waves in accretion disks around compact objects. Astrophys. J. **457**, 805 (1996). https://doi.org/10.1086/176775. arXiv:astro-ph/9508022 [astro-ph]

Nagakura, H., Yamada, S.: The standing accretion shock instability in the disk around the Kerr black hole. Astrophys. J. **696**(2), 2026–2035 (2009). https://doi.org/10.1088/0004-637X/696/2/2026. arXiv:0901.4053 [astro-ph.HE]

Nandi, A., Manickam, S.G., Rao, A.R., et al.: On the source of quasi-periodic oscillations of the black hole candidate GRS 1915 + 105: some new observations and their interpretation. Mon. Not. R. Astron. Soc. **324**(1), 267–272 (2001). https://doi.org/10.1046/j.1365-8711.2001.04339.x. arXiv:astro-ph/0012527 [astro-ph]

Nandi, A., Debnath, D., Mandal, S., et al.: Accretion flow dynamics during the evolution of timing and spectral properties of GX 339-4 during its 2010-11 outburst. Astron. Astrophys. **542**, A56 (2012). https://doi.org/10.1051/0004-6361/201117844. arXiv:1204.5044 [astro-ph.HE]

Nandi, A., Mandal, S., Sreehari, H., et al.: Accretion flow dynamics during 1999 outburst of XTE J1859 + 226—modeling of broadband spectra and constraining the source mass. Astrophys. Space Sci. **363**(5), 90 (2018). https://doi.org/10.1007/s10509-018-3314-1. arXiv:1803.08638 [astro-ph.HE]

Narayan, R., Yi, I.: Advection-dominated accretion: a self-similar solution. Astrophys. J. Lett. **428**, L13 (1994). https://doi.org/10.1086/187381. arXiv:astro-ph/9403052 [astro-ph]

Nayakshin, S.: Corona energy budget in AGN and GBHC's. In: Ferland, G., Baldwin, J. (eds.) Quasars and Cosmology, p. 43 (1999). https://doi.org/10.48550/arXiv.astro-ph/9812109. arXiv:astro-ph/9812109

Okuda, T., Das, S.: Unstable mass-outflows in geometrically thick accretion flows around black holes. Mon. Not. R. Astron. Soc. **453**(1), 147–156 (2015). https://doi.org/10.1093/mnras/stv1626. arXiv:1507.04326 [astro-ph.HE]

Patra, S., Majhi, B.R., Das, S.: Properties of accretion flow in deformed Kerr spacetime. Phys. Dark Universe **37**, 101120 (2022). https://doi.org/10.1016/j.dark.2022.101120. arXiv:2202.10863 [astro-ph.HE]

Peitz, J., Appl, S.: Viscous accretion discs around rotating black holes. Mon. Not. R. Astron. Soc. **286**(3), 681–695 (1997). https://doi.org/10.1093/mnras/286.3.681. arXiv:astro-ph/9612205 [astro-ph]

Penna, R.F., McKinney, J.C., Narayan, R., et al.: Simulations of magnetized discs around black holes: effects of black hole spin, disc thickness and magnetic field geometry. Mon. Not. R. Astron. Soc. **408**(2), 752–782 (2010). https://doi.org/10.1111/j.1365-2966.2010.17170.x. arXiv:1003.0966 [astro-ph.HE]

Penna, R.F., Sadowski, A., McKinney, J.C.: Thin-disc theory with a non-zero-torque boundary condition and comparisons with simulations. Mon. Not. R. Astron. Soc. **420**(1), 684–698 (2012). https://doi.org/10.1111/j.1365-2966.2011.20084.x. arXiv:1110.6556 [astro-ph.HE]

Penna, R.F., Sadowski, A., Kulkarni, A.K., et al.: The Shakura-Sunyaev viscosity prescription with variable α (r). Mon. Not. R. Astron. Soc. **428**(3), 2255–2274 (2013). https://doi.org/10.1093/mnras/sts185. arXiv:1211.0526 [astro-ph.HE]

Porth, O., Chatterjee, K., Narayan, R., et al.: The event horizon general relativistic magnetohydrodynamic code comparison project. Astrophys. J. Suppl. Ser. **243**(2), 26 (2019). https://doi.org/10.3847/1538-4365/ab29fd. arXiv:1904.04923 [astro-ph.HE]

Riffert, H., Herold, H.: Relativistic accretion disk structure revisited. Astrophys. J. **450**, 508 (1995). https://doi.org/10.1086/176161

Sano, T., Inutsuka, S., Turner, N.J., et al.: Angular momentum transport by magnetohydrodynamic turbulence in accretion disks: gas pressure dependence of the saturation level of the magnetorotational instability. Astrophys. J. **605**(1), 321–339 (2004). https://doi.org/10.1086/382184. arXiv:astro-ph/0312480 [astro-ph]

Sarkar, B., Das, S.: Dynamical structure of magnetized dissipative accretion flow around black holes. Mon. Not. R. Astron. Soc. **461**(1), 190–201 (2016). https://doi.org/10.1093/mnras/stw1327. arXiv:1606.00526 [astro-ph.HE]

Sen, G., Maity, D., Das, S.: Study of relativistic accretion flow around KTN black hole with shocks. J. Cosmol. Astropart. Phys. **2022**(8), 048 (2022). https://doi.org/10.1088/1475-7516/2022/08/048. arXiv:2204.02110 [astro-ph.HE]

Shakura, N.I., Sunyaev, R.A.: Reprint of 1973A&A....24..337S. Black holes in binary systems. Observational appearance. Astron. Astrophys. **500**, 33–51 (1973)

Shapiro, S.L., Teukolsky, S.A.: Black Holes, White Dwarfs, and Neutron Stars. The Physics of Compact Objects. Wiley-Interscience, New York (1983)

Smak, J.: Dwarf nova outbursts. III. The viscosity parameter alpha. Acta Astron. **49**, 391–401 (1999)

Smith, D.M., Heindl, W.A., Markwardt, C.B., et al.: A transition to the soft state in GRS 1758-258. Astrophys. J. Lett. **554**(1), L41–L44 (2001). https://doi.org/10.1086/320928. arXiv:astro-ph/0103381 [astro-ph]

Smith, D.M., Heindl, W.A., Swank, J.H.: Two different long-term behaviors in black hole candidates: evidence for two accretion flows? Astrophys. J. **569**(1), 362–380 (2002). https://doi.org/10.1086/339167. arXiv:astro-ph/0103304 [astro-ph]

Sorathia, K.A., Reynolds, C.S., Stone, J.M., et al.: Global simulations of accretion disks. I. Convergence and comparisons with local models. Astrophys. J. **749**(2), 189 (2012). https://doi.org/10.1088/0004-637X/749/2/189. arXiv:1106.4019 [astro-ph.HE]

Sreehari, H., Nandi, A., Das, S., et al.: AstroSat view of GRS 1915 + 105 during the soft state: detection of HFQPOs and estimation of mass and spin. Mon. Not. R. Astron. Soc. **499**(4), 5891–5901 (2020). https://doi.org/10.1093/mnras/staa3135. arXiv:2010.03782 [astro-ph.HE]

Steinacker, A., Papaloizou, J.C.B.: Three-dimensional magnetohydrodynamic simulations of an accretion disk with star-disk boundary layer. Astrophys. J. **571**(1), 413–428 (2002). https://doi.org/10.1086/339892. arXiv:astro-ph/0201479 [astro-ph]

Suková, P., Janiuk, A.: Oscillating shocks in the low angular momentum flows as a source of variability of accreting black holes. Mon. Not. R. Astron. Soc. **447**(2), 1565–1579 (2015). https://doi.org/10.1093/mnras/stu2544. arXiv:1411.7836 [astro-ph.HE]

Sunyaev, R.A., Titarchuk, L.G.: Comptonization of X-rays in plasma clouds – typical radiation spectra. Astron. Astrophys. **86**, 121 (1980)

Yang, R., Kafatos, M.: Shock study in fully relativistic isothermal flows. II. Astron. Astrophys. **295**, 238–244 (1995)

Zhu, Z., Stone, J.M.: Global evolution of an accretion disk with a net vertical field: coronal accretion, flux transport, and disk winds. Astrophys. J. **857**(1), 34 (2018). https://doi.org/10.3847/1538-4357/aaafc9. arXiv:1701.04627 [astro-ph.EP]